Folding, Stowage and Deployment of Viscoelastic Tape Springs

Kawai Kwok[1] and Sergio Pellegrino[2]
California Institute of Technology, Pasadena, CA 91125, United States

This paper presents an experimental and numerical study of the folding, stowage, and deployment behavior of viscoelastic tape springs. Experiments show that during folding the relationship between load and displacement is nonlinear and varies with rate and temperature. In particular, the limit and propagation loads increase with the folding rate but decrease with temperature. During stowage, relaxation behavior leads to a reduction in internal forces that significantly impacts the subsequent deployment dynamics. The deployment behavior starts with a short, dynamic transient that is followed by a steady deployment and ends with a slow creep recovery. Unlike elastic tape springs, localized folds in viscoelastic tape springs do not move during deployment. Finite element simulations based on a linear viscoelastic constitutive model with an experimentally determined relaxation modulus are shown to accurately reproduce the experimentally observed behavior, and to capture the effects of geometric nonlinearity, time and temperature dependence.

---

[1] Graduate Researcher, Graduate Aerospace Laboratories, 1200 E. California Blvd. MC 301-46. AIAA Member. Currently at: Department of Energy Conversion and Storage, Technical University of Denmark, Frederiksborgvej 399, 4000 Roskilde, Denmark
[2] Joyce and Kent Kresa Professor of Aeronautics and Professor of Civil Engineering, Graduate Aerospace Laboratories, 1200 E. California Blvd. MC 301-46. AIAA Fellow. sergiop@caltech.edu

Nomenclature

a_T = temperature shift factor

c_1, c_2 = constants in WLF equation

E = uniaxial relaxation modulus

E_∞ = uniaxial long-term modulus

G = shear relaxation modulus

h = tape spring thickness

$\bar{h}$ = average tape spring thickness

I = second moment of area

K = bulk relaxation modulus

L = tape spring length

M = bending moment

P = reaction force

R = tape spring radius

r = longitudinal radius of curvature of localized fold

T = temperature

T_0 = reference temperature

t = time

t' = reduced time

u = vertical displacement

$\dot{u}$ = vertical displacement rate

v = horizontal displacement

x = horizontal coordinate

α = tape spring subtended angle

ϵ = strain

κ_l = longitudinal curvature

ν = Poisson's ratio

ρ = relaxation times

σ = stress

θ = rotation angle

I. Introduction

Stored strain energy deployable structures built around the concept of the steel tape measure are known as *tape springs*. Tape springs are thin shells with a curved section, typically of uniform curvature and subtending angles smaller than 180°, as shown in Fig. 1. They are particularly suitable for packaging because their curved transverse cross-section can be flattened and then the structure can be easily coiled longitudinally. This process is nearly inextensional and hence dominated by bending strain energy, which is small in a thin structure. Tape springs have been extensively used in deployable booms [1, 2]; also, their ability to form localized elastic folds, as shown in Fig. 2, has been exploited in various deployable structures concepts able to self-deploy and self-lock.

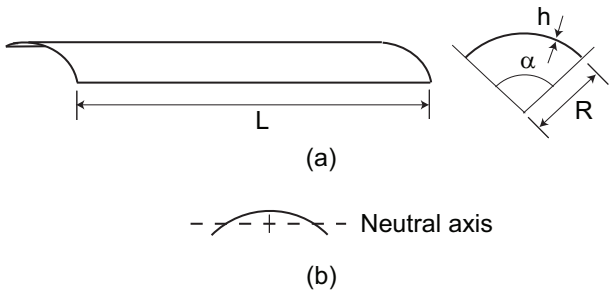

Fig. 1 (a) Tape spring geometry, and (b) neutral axis of cross section.

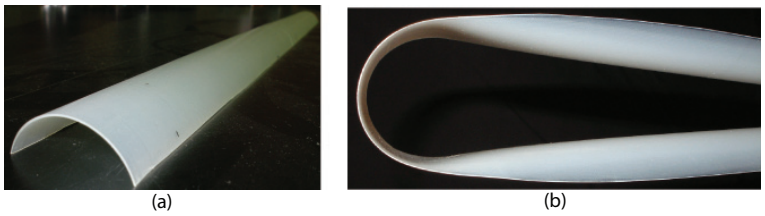

Fig. 2 Tape spring made of LDPE having a radius of 19 mm and a subtended angle of 150°: (a) deployed and (b) folded.

Tape-springs used in deployable space structures have traditionally been made of metallic materials, but recently there has been rising interest in designing tape springs made of reinforced polymer composites because of their low thermal expansion and high specific stiffness [3, 4]. In this case the deployment behavior is dependent on time and temperature due to the viscoelasticity of the matrix. For example, the initial deployment anomaly of the composite booms forming the antennas of the

Mars Express Spacecraft was attributed to the loss of deployment moment after long term stowage [5, 6]. Related experimental studies found that the deployed shape precision and vibration characteristics are also affected by time and temperature effects [7, 8]. As deployable space structures are stowed for extended periods and subjected to varying temperature environments, viscoelastic effects need to be considered for designing deployable structures with predictable deployment behavior and final shape precision.

The present study examines the time and temperature dependent behavior of homogeneous linear viscoelastic tape springs during the folding, stowage and deployment processes. The broad objective is to gain a fundamental understanding of viscoelastic behavior of polymer-based deployable structures and to establish methods of analysis for viscoelastic thin shells.

The material chosen is low density polyethylene (LDPE). While the mechanical properties of polymers depends on their particular molecular structure that gives rise to the distinction between thermosets and thermoplastics, their phenomenological viscoelastic behavior is adequately represented by the same constitutive model above the glass transition temperature. In other words, the moduli of LDPE and epoxies commonly used in composites relax with time in a similar manner provided that the behavior of each material is referenced to its respective glass transition temperature, although in epoxies aging may also need to be modeled.[9, 10] Typical epoxies have glass transition temperatures above 100°C and performing experiments involving large displacements, such as dynamic deployment, at such temperatures is challenging. By choosing LDPE, whose glass transition is below 0° [11], we can study viscoelastic effects near room temperature and the results are indicative of thermosets above the glass transition.

The paper is laid out as follows. Section II reviews the relevant literature. Section III describes the experimental procedures and presents the results of two experiments that were conducted. The first experiment examined the quasi-static folding and stowage processes, while the second investigated the dynamic deployment of shells that had been stowed for a period of time. The results of these experiments demonstrate clear evidence of viscoelastic effects on folding, stowage, and deployment. Section IV presents the finite element model used for studying the time and temperature dependent behavior of these shells. The analyses are based on a linear viscoelastic con-

stitutive model with an experimentally determined master curve. Section V compares the predicted load-displacement relationship, relaxation over time, and deployed displacement with the measured responses. Section VI discusses the findings of the study and concludes the paper.

II. Background

The present study involves two related areas of literature, namely geometric nonlinearity in thin shells and viscoelasticity.

The geometrically nonlinear behavior of elastic tape springs subject to bending has been exploited in many deployable structures and is therefore well studied. The key effect, in a tape spring of finite length, is that a gradually increasing bending moment, which induces tension on the edges and compression in the middle, causes the cross section to ovalize. This results in a gradual reduction in the bending stiffness of the tape spring, defined as the slope of the equilibrium path in moment-rotation space. The stiffness becomes zero when a limit moment is reached and at this point the deformation of the tape spring suddenly localizes as it changes shape from smoothly curved to almost straight with an elastic fold in the middle. The fold region is curved longitudinally but straight transversally, Fig. 3, and it is surrounded by regions that are almost straight longitudinally and have the original curvature transversally. Biaxially curved transition regions connect the fold region to the straight parts[12].

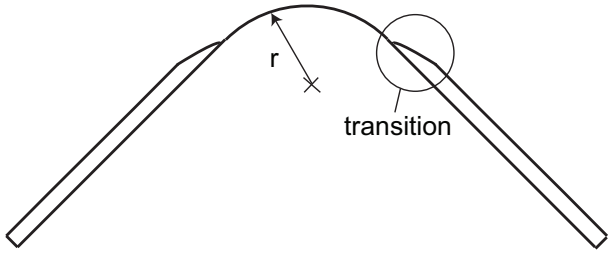

Fig. 3 Configuration of a bent tape spring with three distinct zones of deformation.

The folded tape spring has zero stiffness, as the length of the fold region can be varied under a constant bending moment; the value of this steady-state moment is much lower than the limit moment [13]. This is a characteristic feature of steady-state propagating instabilities in elastic structures and can be captured using a simple energy balance [13–15].

Throughout the entire bending process, the deformation remains elastic and is completely reversible upon removal of the applied moment; this is the principle behind the longitudinal coiling and localized folding of tape springs. Three-dimensional folding, in which tape springs are both bent and twisted, has been proposed for small satellite missions [16, 17].

Polymer-based tape springs exhibit viscoelastic properties and hence their behavior is complicated by time and temperature dependence. The well established and widely used phenomenological theory of viscoelasticity describes the constitutive behavior of polymers with respect to time and temperature [18–21]. In the simplest form of this theory, linear viscoelasticity, the stress-strain relation for uniaxial deformation is expressed in terms of the Boltzmann superposition integral,

$$\sigma(t) = \int_0^t E(t-\tau)\frac{d\epsilon}{d\tau}d\tau, \tag{1}$$

where σ is stress, ϵ is strain, and E is the relaxation modulus that expresses the time variation of the modulus.

For analysis of real materials over a wide range of time scales, an exponential series known as the Prony series is often used to represent the relaxation modulus. The Prony series representation is given by

$$E(t) = E_\infty + \sum_{i=1}^{n} E_i e^{-t/\rho_i}, \tag{2}$$

where t is time, E_∞ is the long-term modulus, E_i are the Prony coefficients, and ρ_i are the corresponding relaxation times. Each exponential term effectively represents the variation of the relaxation modulus within 1 decade of time. The terms in the Prony series that are required for a specific analysis depend upon the time range of interest. Relaxation and creep tests are the fundamental characterization methods for obtaining the relaxation modulus, however, extended testing periods are required for measuring the long-term response if the tests are conducted at a single temperature.

For polymers, there exists a remarkable relationship between time and temperature, known as the time-temperature superposition principle, which provides a means to study long-term behavior of viscoelastic materials using short-term characterization tests. The key idea is to postulate a shift factor a_T which is the ratio of relaxation times at two different temperatures [20],

$$a_T = \frac{\rho(T)}{\rho(T_0)}, \tag{3}$$

where ρ is the relaxation time and T_0 is some reference temperature. As indicated earlier, a polymer has many relaxation times. If the same shift factor applies to all relaxation times, the polymer is termed thermorheologically simple. A widely used empirical relation for a_T is the Williams-Landel-Ferry (WLF) equation [22],

$$\log a_T = -\frac{c_1(T - T_0)}{c_2 + (T - T_0)}, \tag{4}$$

in which c_1 and c_2 are material constants that depend on the particular polymer and the logarithm is of base ten.

To relate the effects of time and temperature, the concept of reduced time t' is introduced. It is given by,

$$t' = \int_0^t \frac{d\tau}{a_T(T)}. \tag{5}$$

In the simple case of constant temperature over time, the reduced time becomes

$$t' = \frac{t}{a_T}, \tag{6}$$

and it follows that

$$E_T(t) = E_{T_0}(t'). \tag{7}$$

In essence, the time-temperature superposition principle suggests that the modulus at temperature T and time t is the same as the modulus at the reference temperature T_0 and reduced time t'. Therefore, one can relate the relaxation modulus at one temperature to that at another temperature by a shift in the time scale.

Based on this principle, a master curve for a thermorheologically simple material can be constructed at any arbitrary reference temperature by shifting the relaxation moduli at all other temperatures to the reference temperature. On a log-log plot of relaxation versus time, this is equivalent to a horizontal shift by $\log a_T(T)$. The resulting master curve is a plot of relaxation modulus that describes both the time and temperature dependence of the material behavior. In terms of reduced time, the constitutive relation, Eq. (1), is given by

$$\sigma(t) = \int_0^{t'} E(t' - \tau')\frac{d\epsilon}{d\tau}d\tau. \tag{8}$$

III. Experiments

This section first describes the specimen fabrication and characterization processes, and then presents the procedures and results of two experiments. The first experiment investigated the folding-stowage process with careful control and measurement of load and displacement over time. This test helped develop an understanding of the tape spring deformation prior to deployment. The second experiment measured continuously the response of the tape spring during folding, stowage and deployment, but focused on analyzing the final deployment and shape recovery behavior.

A. Fabrication of Tape Springs

Tape spring specimens were fabricated from a single flat LDPE sheet obtained from the United States Plastic Corporation, through a thermal remolding process. The LDPE sheet stock had a length of 610 mm, a width of 914 mm, and a thickness of 0.79 mm. A strip of LDPE was cut to the required length, sandwiched between two release fabric layers, wrapped around a cylindrical steel mandrel, restrained with heat shrink tape, and subject to a thermal cycle. The assembly was heated to 120°C, maintained at this temperature for 4 hours, and then allowed to cool to room temperature in 8 hours at a constant cooling rate inside an oven with a temperature control precision of ±2°C. The long heating and cooling periods allowed enough time for LDPE to recrystallize and to minimize the effect of physical aging, respectively. To further eliminate the effects of physical aging, the fabricated specimen was kept at room temperature for another 24 hours before any tests were performed. After this procedure, it was assumed that temporally stable mechanical properties had been achieved in the remolded material.

The specimen was cut into two pieces and different experiments were conducted on each piece, see Table 1, in which $\bar{h}$ denotes the average thickness of the shell. The measured radius was higher than that of the steel mandrel because the shells recoiled by a consistent amount after release from the mold. The thickness variation was measured using an Elcometer 456 coating thickness gauge with a resolution of 10 microns. A rectangular grid was drawn on each specimen and the thickness at the grid points was measured. The grid spacing was 16 mm along the length and 10 mm along the circumference of the tape spring. The thickness contours of the specimen used in the folding-stowage

experiment are shown in Fig. 4.

Experiment	L $[mm]$	R $[mm]$	$\bar{h}$ $[mm]$	α [deg]
Folding-Stowage	272.0	19.0	0.73	150
Deployment-Recovery	398.0	19.0	0.73	150

Table 1 Dimensions of tape springs.

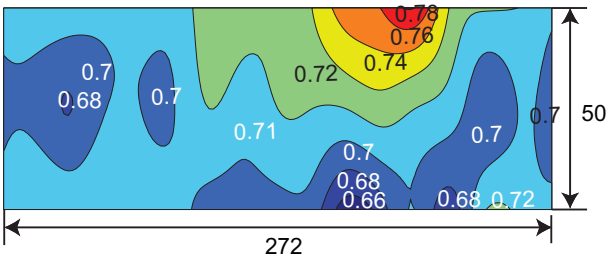

Fig. 4 Thickness distribution, in millimeters, of tape spring specimen used in folding-stowage experiment. The vertical coordinate is the cross-sectional arc-length.

B. Master Curve of LDPE

The relaxation modulus of LDPE was characterized through a series of uniaxial tension relaxation tests. Three rectangular test coupons with a length of 165 mm and a width of 40.0 mm were cut from a LDPE sheet with a thickness of 1.56 mm, which had been previously subjected to the same remolding process of the tape springs. Tests were performed inside an environmental chamber (Instron Heatwave Model 3119-506) utilizing a built-in thermocouple to control the temperature with a precision of $\pm 1°C$. A type-T thermocouple made of Copper/Constantan was attached to the surface of a dummy LDPE coupon close to the test coupon. The stability of the temperature conditioning inside the environmental chamber was measured by prescribing a temperature impulse and recording the subsequent temperature variation over time both with the built-in thermocouple and the dummy coupon thermocouple. It was found that the temperature readings from the two thermocouples became identical 30 minutes after the impulse. This indicates that thermal equilibrium is established within such time frame, and this thermal conditioning time was allowed prior to each test.

Before testing, the temperature was brought to the specified value and the coupon was thermally conditioned for 30 minutes at the test temperature. Because of the viscoelastic nature of LDPE, the observed load changed over time after the application of the preload. Therefore, the test coupon was allowed to rest until the observed load reached a steady value.

The coupons were tested at $0°C$, $10°C$ and $22°C$, and at each of these temperatures the test on the same coupon was repeated three times. Each test consisted in stretching the coupon to a strain of 0.005 in 1 second and this strain was held constant for 3 hours. The longitudinal and transverse strains in the coupon were measured using two laser extensometers (Electronic Instrument Research Ltd LE-05) with a recording rate of 5 Hz.

The averages of the measured relaxation moduli are presented in Fig. 5. The initial portion of the relaxation test data after loading with a finite strain rate deviates from that in the case of ideal instantaneous straining. The difference becomes negligible in about 10 times the loading time[24]. For this reason, the data obtained during the first 10 s after loading were discarded. The individual relaxation moduli at $T = 0°C$ and $T = 10°C$ were shifted with respect to the reference temperature of $T_0 = 22°C$ to form a master curve. The corresponding shift factors were determined so that the shifted relaxation moduli and the unshifted one at T_0 lie along a single smooth curve. Figure 6 shows the master curve of LDPE at the reference temperature.

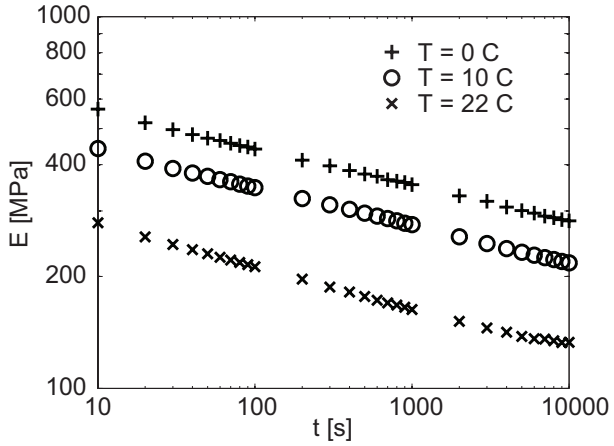

Fig. 5 Relaxation moduli versus time at test temperatures

The long term modulus, Prony coefficients and relaxation times were determined by fitting the

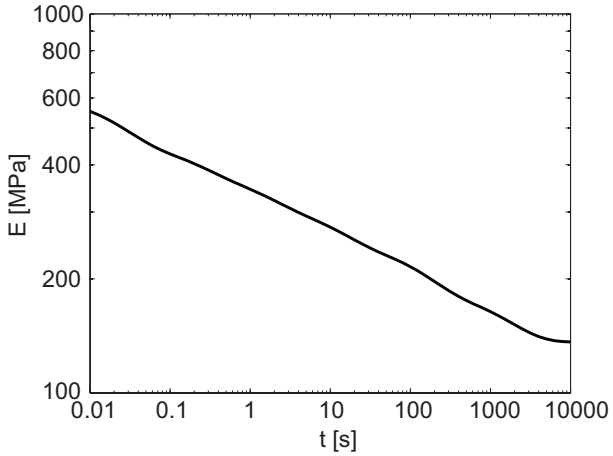

Fig. 6 Master curve for LDPE at $22^{\circ}C$

i	E_i $[MPa]$	ρ_i [s]
∞	136.2	—
1	150.6	2.43×10^{-2}
2	74.81	2.17×10^{-1}
3	68.26	1.52
4	65.22	1.24×10
5	62.85	1.49×10^{2}
6	49.83	1.69×10^{3}

Table 2 Prony series parameters for LDPE

Prony series representation, Eq. (2), to the master curve using the Levenberg-Marquardt optimization algorithm in Matlab. Table 2 lists the parameters of the 6-term Prony series that was obtained. Similarly, the material constants c_1 and c_2 were found by fitting the temperature shift data to the WLF equation, Eq. (4), and the values obtained were

$$c_1 = -8.74 \quad \text{and} \quad c_2 = -40.41^{\circ}\text{C}$$

C. Folding-Stowage Experiments

The folding-stowage sequence was implemented by bending a tape spring to a prescribed end rotation and holding the rotation angle fixed over time. The tape spring was bent in an opposite

sense (i.e. the longitudinal and transverse curvature changes have opposite signs) by applying an eccentric compression on the end cross sections. To allow the end cross sections to deform and freely rotate during folding, the mid-point of each end cross section was placed in contact with a thin aluminum plate attached to the load frame. Prior to starting the test, the tape spring was held upright by means of a small compressive preload applied through the two contact points between the aluminum plates and the tape spring. The test configuration is schematically shown in Fig. 7. The procedure adopted in the present experiment allows full control of the boundary conditions and also precise tracking of the load and displacement histories over time, which is important for achieving repeatable measurements in the present path dependent problem.

Tests were carried out in displacement-controlled mode following the same procedures described in Sec. III B. In each test, a downward displacement of 80 mm was applied and then the tape spring was held in this final configuration for 5000 s. Two temperatures, $T = 15°\text{C}$ and $22°\text{C}$, and two displacement rates, $\dot{u} = 1$ mm/s and 5 mm/s, were chosen. Full field views of the deformed tape spring were captured continuously using a high-resolution digital camcorder.

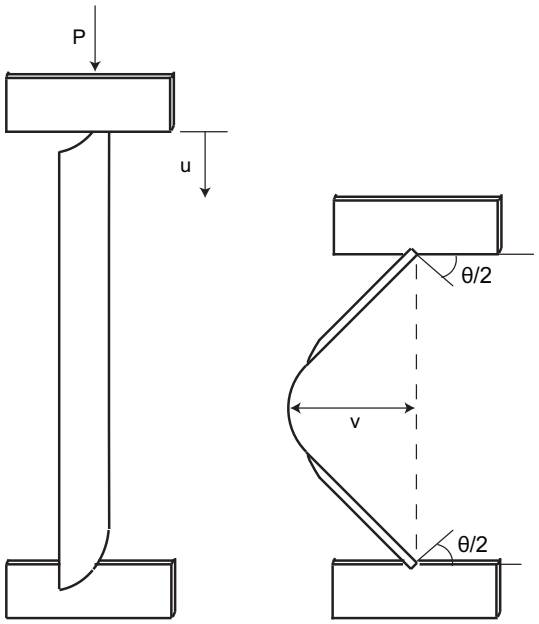

Fig. 7 Schematic of folding-stowage test.

The measured load P and displacement u over time during folding are plotted in Fig. 8. The load response has been converted to a plot of moment M vs. rotation θ in Fig. 9 for the case of

$\dot{u} = 1$ mm/s at $T = 22°$C. The rotation has been obtained by adding the end rotations measured from the images of the deformed specimen, and the moment has been obtained from the measured load multiplied by the distance between the line of action of the load and the middle cross section of the tape spring, v, also measured from the images. Images of the specimen at different stages of the test are shown in Fig. 10. The label of each image corresponds to a specific point in Fig. 9.

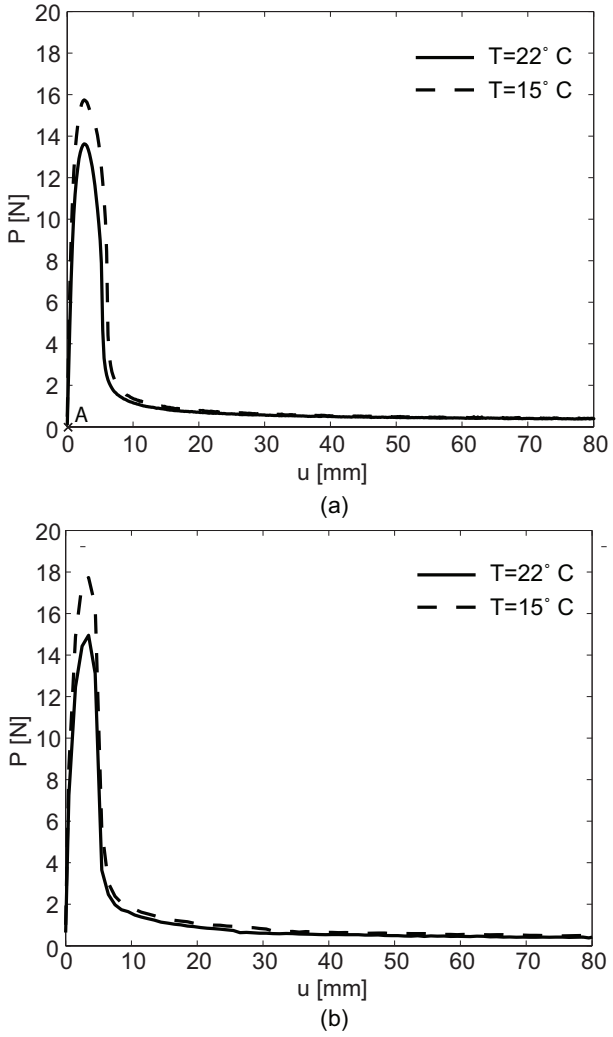

Fig. 8 Measured load response during folding: (a) $\dot{u} = 1$ mm/s and (b) $\dot{u} = 5$ mm/s.

The initial part of the response in Fig. 9 shows a stiff, softening behavior. Then, the tape spring bends uniformly, see configurations A - C in Fig. 10, with a decreasing bending stiffness EI, where I is the second moment of area of the cross section about the neutral axis. This nonlinearity is due to changes in both E and I: first, the second moment of area decreases with rotation as a result

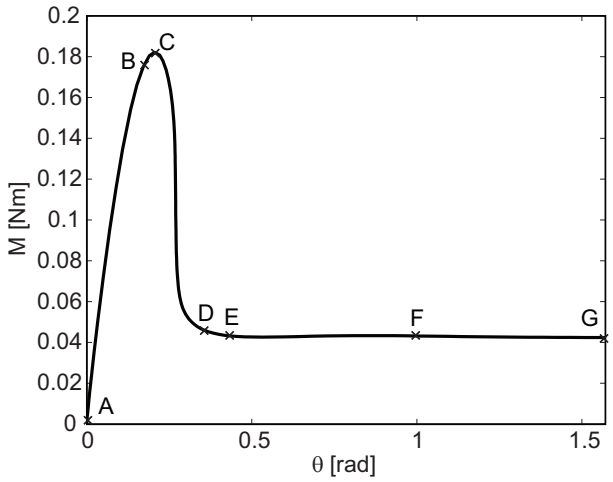

Fig. 9 Measurements of moment vs. rotation for $\dot{u} = 1$ mm/s and $T = 22^{\circ}$C.

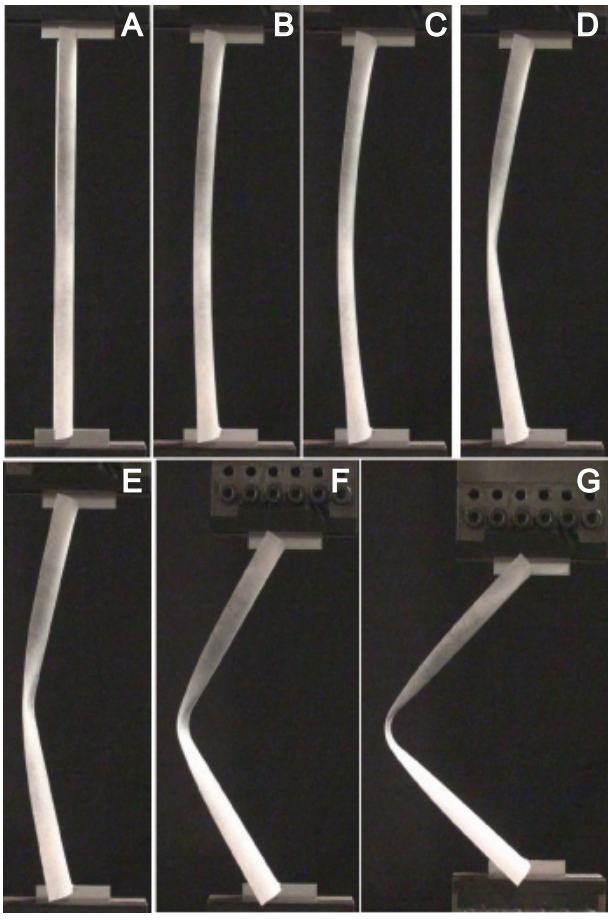

Fig. 10 Sequence of deformed shapes corresponding to the response in Fig. 9.

of ovalization and, second, the longitudinal modulus relaxes with time because of viscoelasticity. In this uniform deformation stage, the longitudinal curvature is given by $\kappa_l = \theta/L$. Uniform bending ceases in the configuration C, which is just past after reaching the maximum moment. At this point, a buckle begins to form in the middle of the tape spring. Although the applied loading is not completely symmetric, due to gravity, but this asymmetry is too small to have a significant impact on the location of the buckle. From configuration C to E, the moment drops sharply as the end rotations continue to increase. This corresponds to an expansion of the buckle in the transverse direction and unloading of the regions away from the buckle. The buckle has fully developed in configuration E, where a localized fold region with zero transverse curvature has been formed. At this stage, the tape spring has adopted the deformation pattern outlined in Fig. 3, with longitudinally curved and straight parts of the tape spring coexisting. From this point onwards, configurations E - G, the moment stays constant with rotation and the fold length increases as a result of the propagation of the localized fold into the straight portions of the tape spring. This fold propagation occurs in a quasi-static manner in the present case because of the displacement-controlled loading mode adopted in this test.

The load responses during folding at two different rates and temperatures have been plotted in Fig. 8. These plots show similar types of nonlinear response, but the maximum load values are different. It can be seen in Fig. 8 that higher maximum loads occur at lower temperatures and faster rates, due to the time and temperature dependence of viscoelastic materials. Their mechanical response is in general nonlinearly affected by rate and temperature, but the stresses are always higher at lower temperatures and faster rates. In Section IV a viscoelastic constitutive model will be employed to analyze such effects in detail.

Load relaxation during stowage is evidenced by plotting the change in load over time on a semi-log scale, Fig. 11. The linearity of the curves from 1000 s to 5000 s on a log time axis implies that the reduction in load is exponential in time. After 5000 s the load has dropped to about one-third of its value at the end of folding. At both rates, higher loads are measured at the lower temperature throughout the entire stowage period.

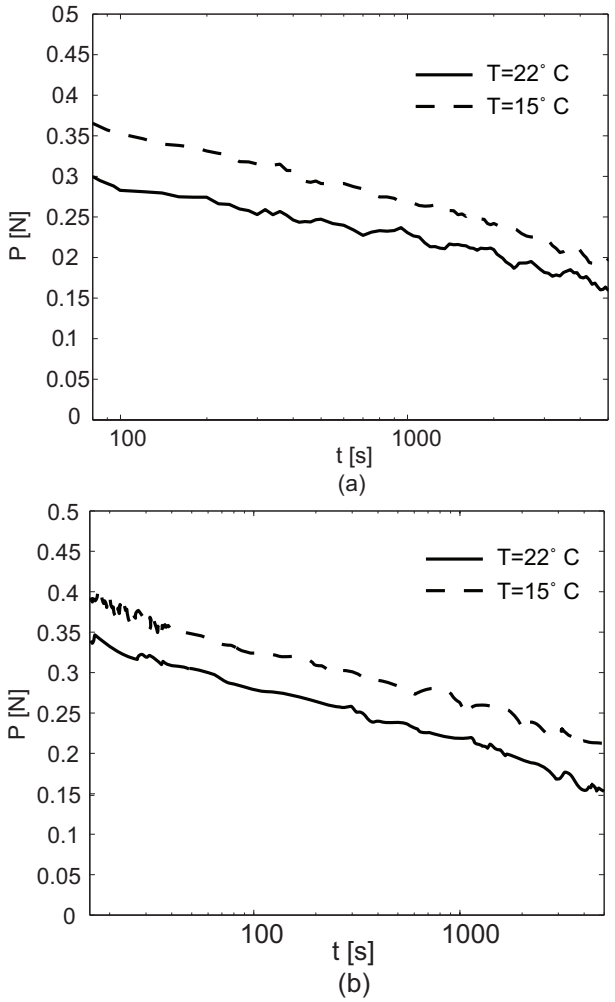

Fig. 11 Measured load relaxation in stowed configuration: (a) $\dot{u} = 1$ mm/s and (b) $\dot{u} = 5$ mm/s.

D. Deployment Experiments

The deployment dynamics were measured using the test configuration shown in Fig. 12. The specimen was clamped at the bottom and held vertical. It was first folded to an angle of 87° over a period of 9 s by manually applying a follower force on the free end; it was then held stowed for 983 s. While in the stowed configuration, the force at the free end was measured by connecting the specimen to a load cell through a cord. Deployment was initiated by cutting the cord at the end of the stowage period. The entire test was carried out at 22°C.

To characterize the deformation, a target point P near the free end was marked (Fig. 12) and its lateral displacement x_p was tracked during deployment. Values of x_p larger than 20 mm were

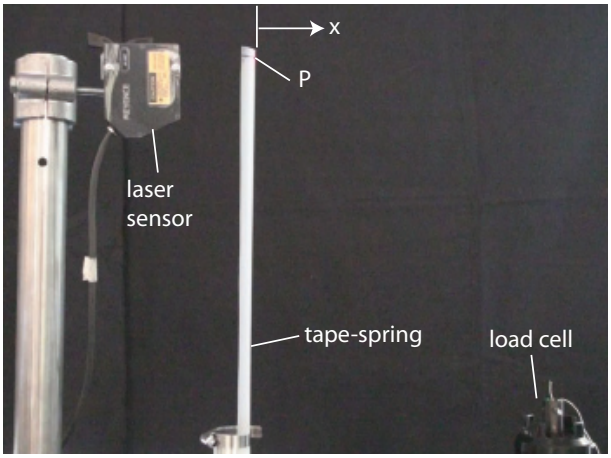

Fig. 12 Deployment test configuration.

extracted from images taken using a high resolution camcorder with a frame rate of 30 fps. For higher accuracy, a laser displacement sensor (Keyence LK-G87) was used to measure values of x_p smaller than 20 mm.

Figure 13 shows a series of snapshots of the deployment sequence. The corresponding values of x_p and t are provided in Fig. 14, which includes three detailed views of the displacement response over time, each highlighting a particular feature. The deployment response can be divided into three stages, each with its own distinctive characteristics. First, a dynamic response is seen during the first 5 s, Fig. 14(b), which includes an oscillation with a period of about 0.8 s about a displacement that decreases over time. Second, the next phase involves a steady deployment that occurs between 5 s and 55 s, Fig. 14(c), with the lateral displacement actually overshooting the deployed configuration by 11 mm. An interesting feature in these first two stages is that the fold does not move: this behavior is different from that of a linear elastic tape spring in which deployment is accompanied by the fold traveling towards the fixed end [13]. Third, a slow creep recovery of the fold cross section leads to a near-zero lateral displacement over a period of 3000 s, Fig. 14(d).

After the test, a close examination of the tape spring revealed that the cross section geometry had not completely recovered, but the magnitude of deformation was too small to be measured precisely with the present experimental setup. The test specimen was monitored visually over three months and the cross section of the fold was found to continue recovering at room temperature in

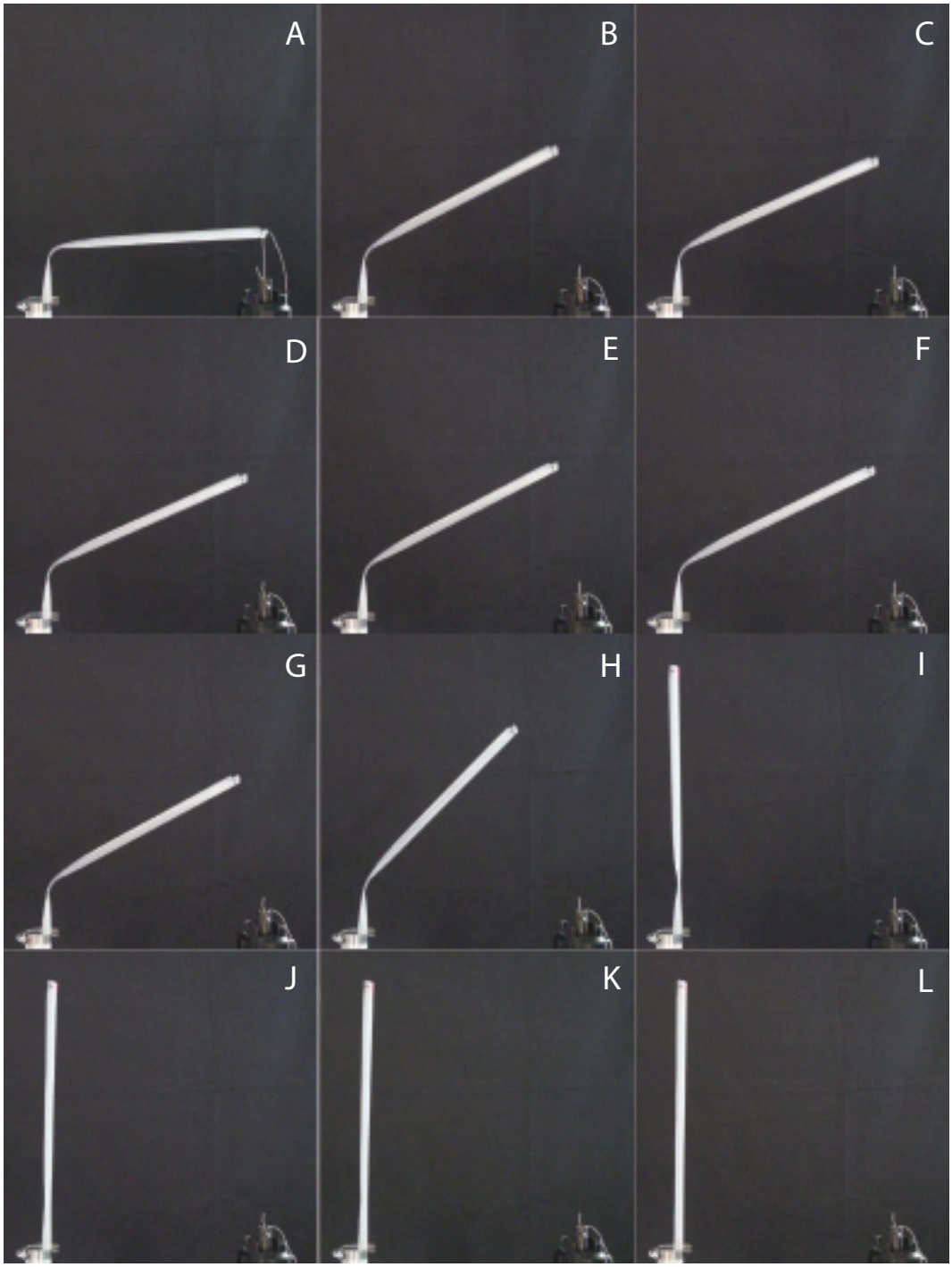

Fig. 13 Deployment sequence: (A)-(F) from 0 s to 2.5 s in steps of 0.5 s, (G)-(I): from 5 s to 55 s in steps of 25 s, and (J)-(L): from 1000 s to 3000 s in steps of 1000 s.

an asymptotic manner.

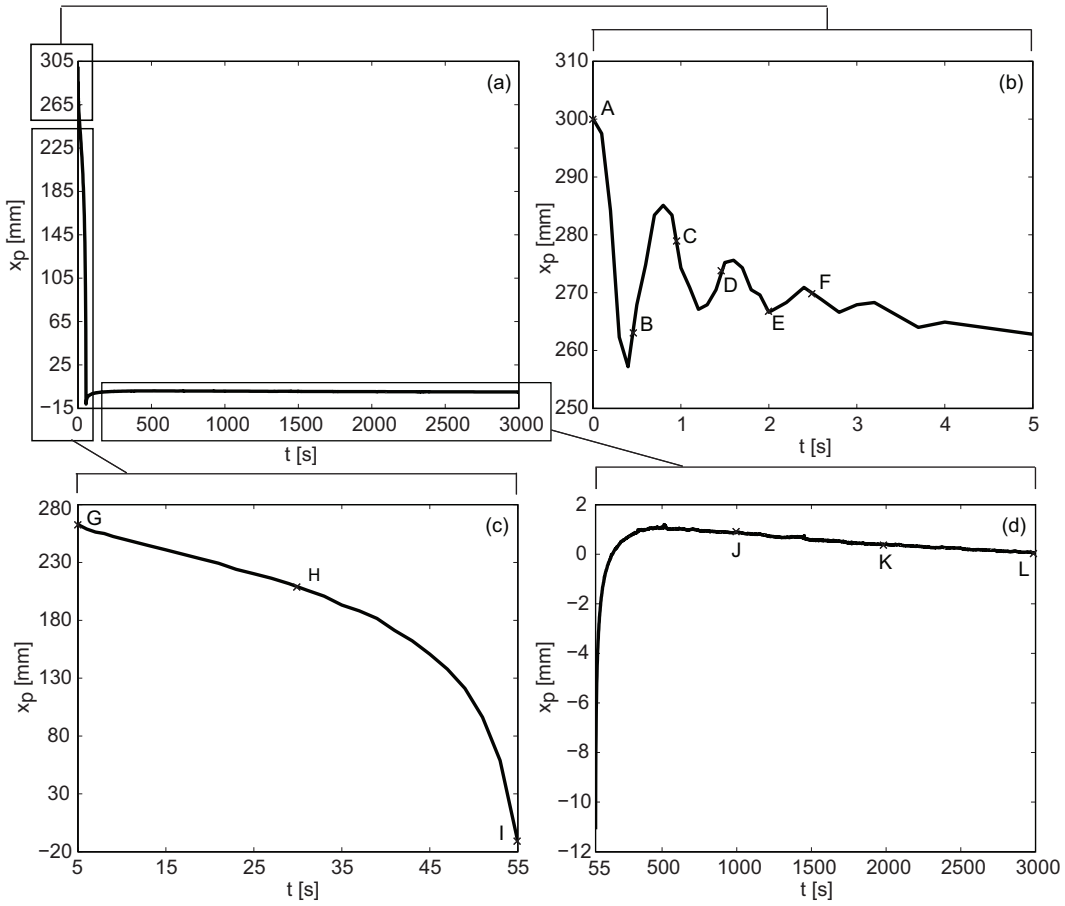

Fig. 14 Measured lateral displacement of point P during deployment: (a) overall behavior; (b) dynamic deployment; (c) steady deployment; (d) creep recovery.

IV. Finite Element Simulations

To investigate the nonlinear behavior of thin shells, including the effects of rate and temperature observed in Sec. III, a finite element analysis was conducted with the finite-element package Abaqus/Standard [23]. A linear viscoelastic constitutive model based on the relaxation modulus of LDPE was used for this study.

A. Finite Element Model

The two tape springs tested in Sec. III were modeled as cylindrical shells as shown in Fig. 15. The model dimensions were as defined in Table 1 and the thickness variation was included in the model by specifying the thickness at each node. The thickness at each node position was determined from the measured thickness distribution using spline interpolation.

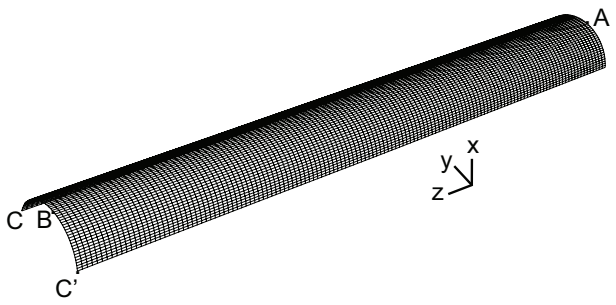

Fig. 15 Finite element model.

For simulating the folding-stowage experiment in Sec. III C, a mesh with 6800 quadrilateral shell elements S4 with a maximum dimension of 2 mm was used. The mesh density in the circumferential direction was twice that in the longitudinal direction for precise computation of the localized fold. Displacement boundary conditions were defined on two nodes, A and B, one on each end section of the shell and coinciding with the mid-point of the cross section. Node B was fully constrained against translation in any direction, whereas the boundary conditions for node A were varied during the simulation, as explained below. Gravity loading was defined over the whole shell, in the positive z direction, throughout the analysis. A geometrically non-linear quasi-static analysis was carried out in two steps, as follows, using the NLGEOM option in Abaqus. An initial folding step, in which a displacement $u_z = 80$ mm was imposed on node A, at the same rates and temperatures used in the experiments. A subsequent stowage step, in which the degrees of freedom of node A were held fixed at the same values as at the end of the folding step. These boundary conditions were held constant for 5000 s. The accuracy of integration in the quasi-static analysis was controlled by specifying the tolerance parameter *CETOL which sets a limit on the maximum change in creep strain rate allowed over a time increment. A value of 1×10^{-4} was found to be adequate for obtaining accurate solutions.

The deployment-recovery test in Sec. III D was analyzed using a mesh with 2500 elements and a maximum dimension of 4 mm. For this simulation, all nodes on the section CC' were fixed and the analysis steps were as follows. In the folding step, a displacement of 300 mm along the x-axis was imposed to node A over a period of 9 s. At the end of the folding step the tape spring had reached the stowed configuration. The displacement of node A along the y-axis was then held fixed

for 983 s in the stowage step, while all other degrees of freedom of node A were left unconstrained. These two steps were carried out quasi-statically. At the end of the stowage step the constraint on node A was instantaneously released and a dynamic analysis was run for 3000 s.

B. Constitutive Model

The constitutive behavior of the shell elements was defined to be linear viscoelastic. Implementation of the Prony series model of Sec. III B in Abaqus/Standard requires the specification of the shear and bulk moduli, which are related to the uniaxial modulus through the equations

$$G(t) = \frac{E(t)}{2(1+\nu)}, \tag{9}$$

$$K(t) = \frac{E(t)}{3(1-2\nu)}, \tag{10}$$

where ν is the Poisson's ratio, G is the shear modulus and K is the bulk modulus. A Poisson's ratio of 0.49 had been determined from the relaxation tests and this value was assumed to be constant in the present study. This assumption implicitly leads to the condition that bulk and shear moduli are synchronous [25]. In general, this is not a realistic description for most materials, however, as shown in Sec. V, this assumption does not seem to have a significant effect on the behavior of the tape spring. The relaxation modulus specified in Table 2 was assigned to the shell elements with the option *VISCOELASTIC, TIME=PRONY.

C. Results

The evolution of the stress distribution as the tape spring is folded, stowed and deployed can be studied with the finite element model. The longitudinal stresses on the outer surface during folding at $T = 22°\text{C}$ with $\dot{u} = 1$ mm/s are shown in Fig. 16. At the beginning, Fig. 16(a), the tape spring is bent smoothly and is under tension on the longitudinal edges. After the instability is initiated, Fig. 16(b), the deformation starts localizing in the middle of the shell and the variation between the edges and the center increases. The buckle subsequently spreads transversely to form a complete fold, which is in uniform compression in the middle but rises rapidly to tension near the edges, Fig. 16(c). Once the localization occurs, the longitudinal stresses are much reduced away from the fold.

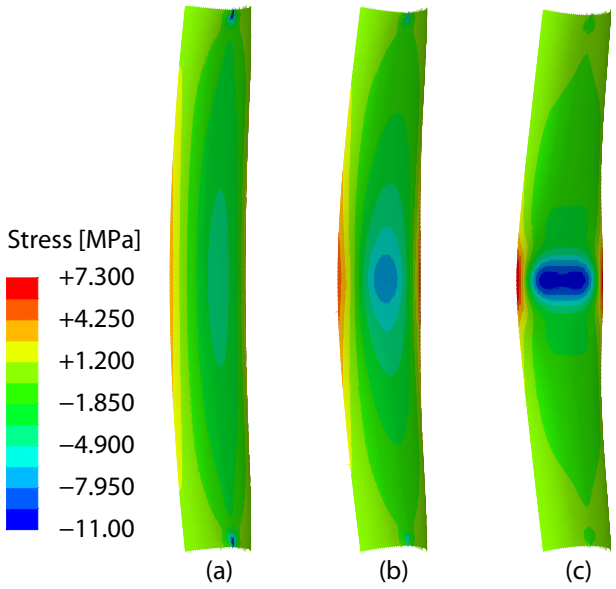

Fig. 16 Longitudinal stresses on outer surface: (a) during initial uniform bending, (b) after instability is initiated and (c) as buckle develops.

Stress relaxation in the stowed state is shown in Fig. 17, which plots the longitudinal stress on the outer shell surface, at the beginning and at the end of the stowage period. Note that the longitudinal stress magnitudes have significantly decreased over the stowage period and the fold region has extended longitudinally. A reduction in the longitudinal curvature of the fold is also predicted by the simulation as the fold region increases in length.

Three intermediate deformed shapes during deployment and the corresponding stress distributions are shown in Fig. 18. In the steady deployment phase, the arclength of the fold decreases while the transverse curvature remains zero. As the tape spring passes through the position with $x_p = 0$ and overshoots, the longitudinal bending stress on the two edges gradually reduces to zero. The longitudinal curvature is practically zero after the overshoot and the remaining part of the deployment is controlled by the recovery of the transverse curvature in the fold. The simulation shows that the fold remains stationary throughout the entire deployment, which agrees with experimental observations.

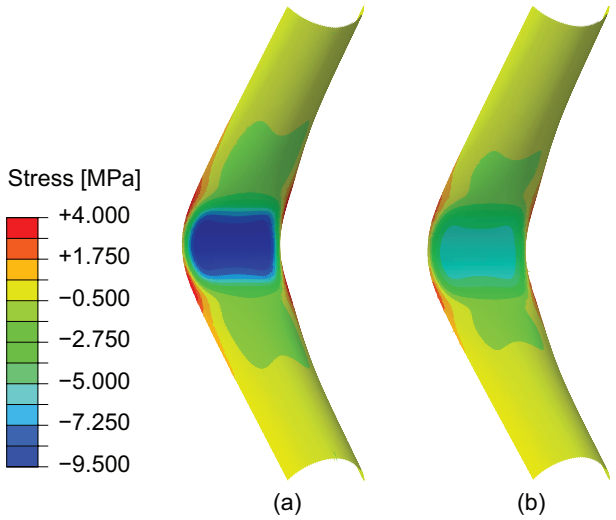

Fig. 17 Relaxation of longitudinal stresses on outer surface: (a) beginning of stowage and (b) end of stowage.

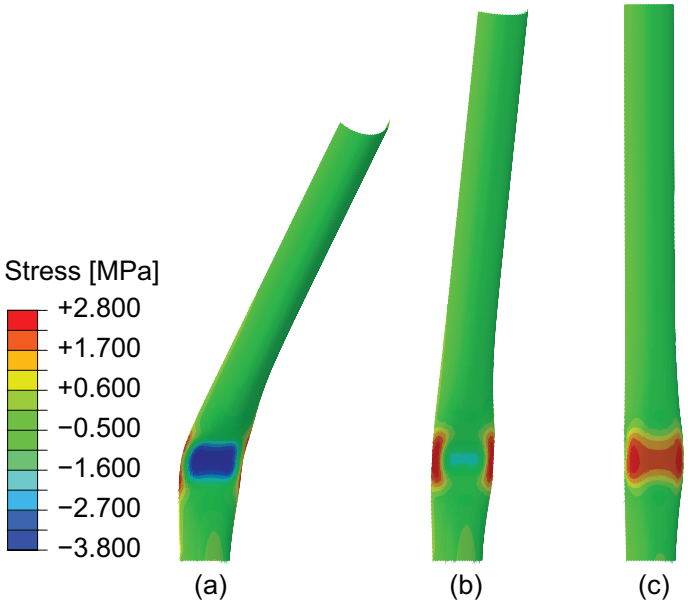

Fig. 18 Longitudinal stress on outer surface: (a) steady deployment (b) passing through $x_p = 0$ and (c) maximum overshoot configuration.

V. Comparison of Experimental and Finite Element Results

Both quantitative and qualitative comparisons between simulations and experiments are presented in this section. Starting from the folding test, the calculated load versus time responses for the case $\dot{u} = 1$ mm/s and two different temperatures are plotted along with the corresponding

experimental measurements in Fig. 19. The predicted response is found to match the observed response in all aspects. The initial stiffness, onset of limit load instability, and postbuckling load plateau are all well reproduced. Only minor discrepancies are found in the values of the buckling load, which is overpredicted by 0.9 N and 0.3 N for temperatures of 15°C and 22°C respectively. These errors are likely due to additional geometric imperfections that were not characterized in the study, such as non-uniformity of the cross section shape along the length of the tape spring. These discrepancies are however insignificant in magnitude. Four deformed configurations during folding stage are compared in Fig. 20. Both the evolution of the overall deformed geometry and the shape of the localized fold are closely captured by the simulation.

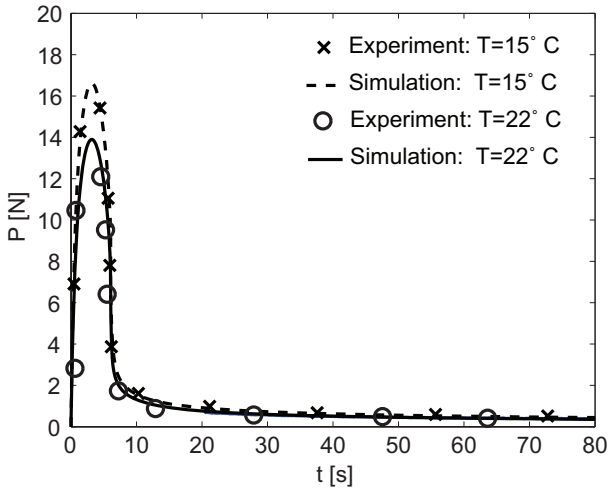

Fig. 19 Comparison of load vs. time during folding, for $\dot{u} = 1$ mm/s.

Next, consider the stowage tests. The load relaxation responses in the stowed configuration for two different temperatures and a folding rate of $\dot{u} = 1$ mm/s are plotted in Fig. 21. Predicted and measured responses are in good agreement, indicating that the finite element model is accurate for long term simulations.

Finally, consider the deployment tests. The lateral displacements x_p are compared in Fig. 22 and it is found that all features of the response have been reproduced by the simulation with only minor discrepancies. In the initial dynamic phase, Fig. 22(a), the predicted oscillations are essentially over in 4 s, which is slightly earlier than the measured response. A small discrepancy is also found in the steady deployment phase, Figure 22(b), as the simulation predicts the maximum overshoot to occur

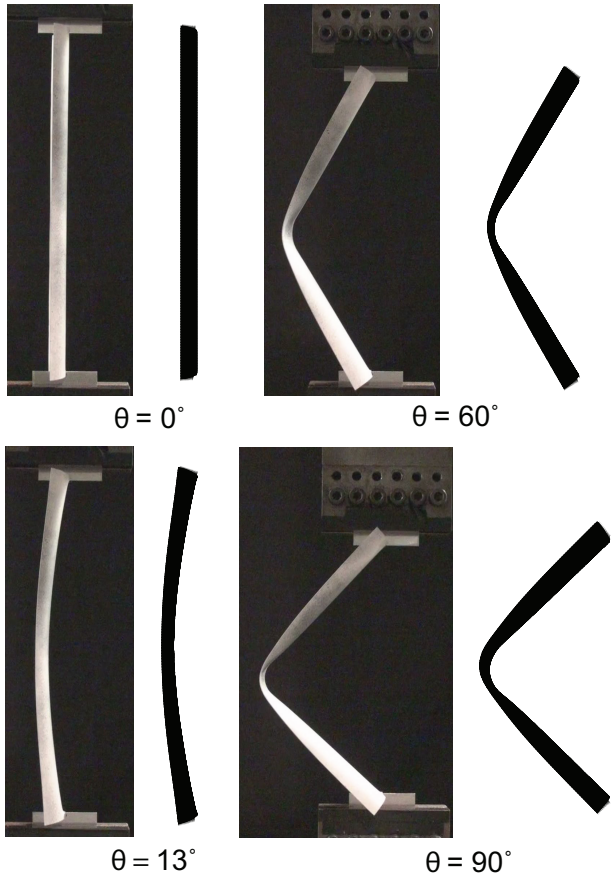

Fig. 20 Comparison of deformed shapes during folding and stowage.

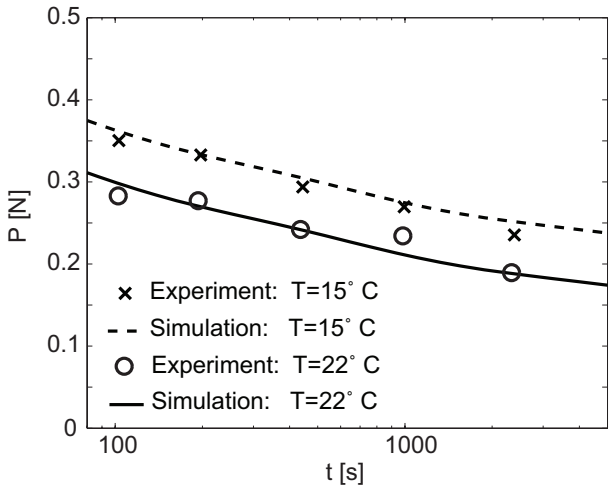

Fig. 21 Comparison of load vs. time during stowage, for $\dot{u} = 1$ mm/s.

2.5 s earlier than observed in the experiment. Nonetheless, the long term creep recovery is well predicted, Fig. 22(c), with a discrepancy of less than 1 mm by the end of the simulation, at 3000 s. A comparison of deployed shapes is provided in Fig. 23, which demonstrates good correlation in the dynamics of the fold. The main source of the discrepancies outlined above is believed to be variations in environmental conditions during the deployment experiments.

VI. Conclusion

Cylindrical thin-shell structures, known as tape springs, are widely used in deployable structures. If made of polymeric materials, they exhibit nonlinear geometric, time and temperature dependent behavior when they are subject to bending. The present study was the first to examine viscoelastic effects during folding, stowage, and deployment of tape springs.

Viscoelastic tape springs can be folded by triggering a local instability and the resulting nonlinear load-displacement relationship is characterized by a limit load and a propagation load. Both of these loads increase with the folding rate but decrease with temperature. Stress relaxation occurs during stowage, and there is a corresponding reduction over time of the instantaneous spring-back upon release that initiates deployment of the tape spring.

The deployment behavior of tape springs that have been held stowed for a period of time encompasses three distinct stages. The first stage is a dynamic response accompanied by a low magnitude vibration. This short dynamic phase is followed by a steady deployment in which the tape spring returns towards the original, straight deployed configuration and overshoots by a small amount. The third phase is a slow creep recovery of the fold cross section, accompanied by an asymptotic recovery of the original position of the tip of the tape spring. A unique feature of viscoelastic tape springs is that the folds remain stationary throughout deployment, whereas in elastic tape springs, which show a much stronger dynamic response, localized folds travel along the tape spring during deployment [13]. This difference is due to the inherent energy dissipation in viscoelastic structures. Because of load relaxation, the energy stored during folding of the tape spring is dissipated over time and the internal force becomes too low to cause significant dynamics. An advantage of this effect is that the deployment process becomes more steady and the risk of

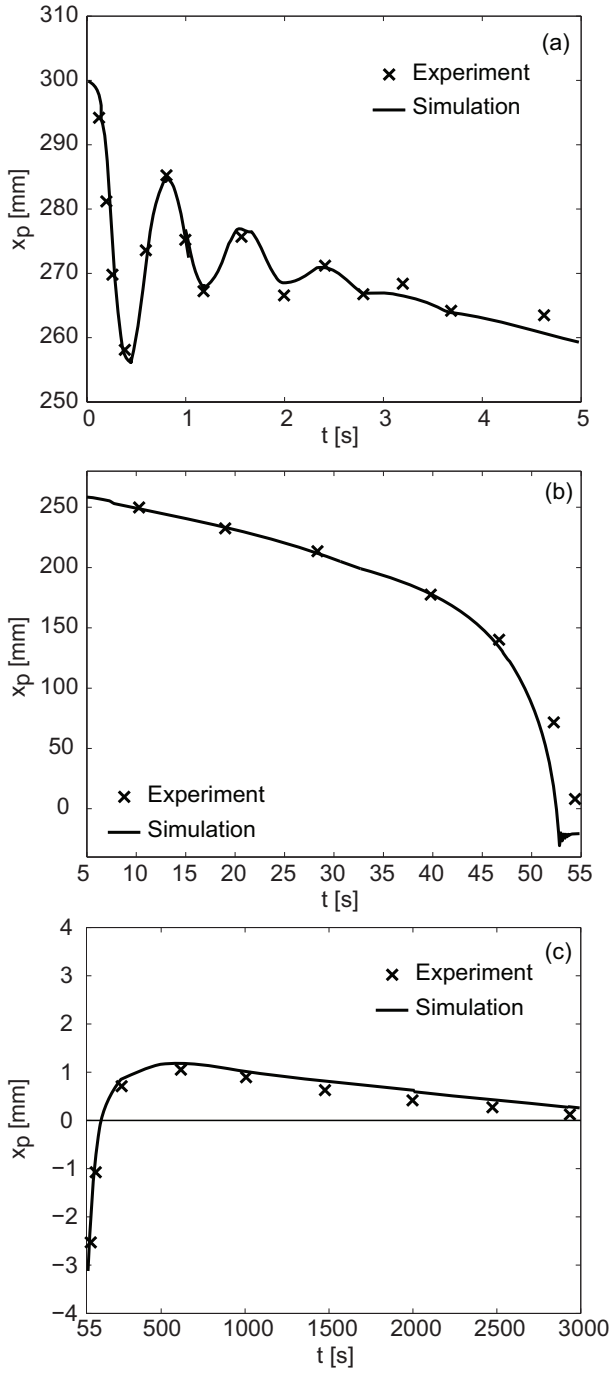

Fig. 22 Comparison of lateral displacement of shell free end: (a) transient dynamic response, (b) steady deployment and (c) long term creep recovery.

damage due to dynamic events is decreased. However, the internal force may become so small that even a small resistance to deployment may be sufficient to prevent the structure from ever reaching the original configuration.

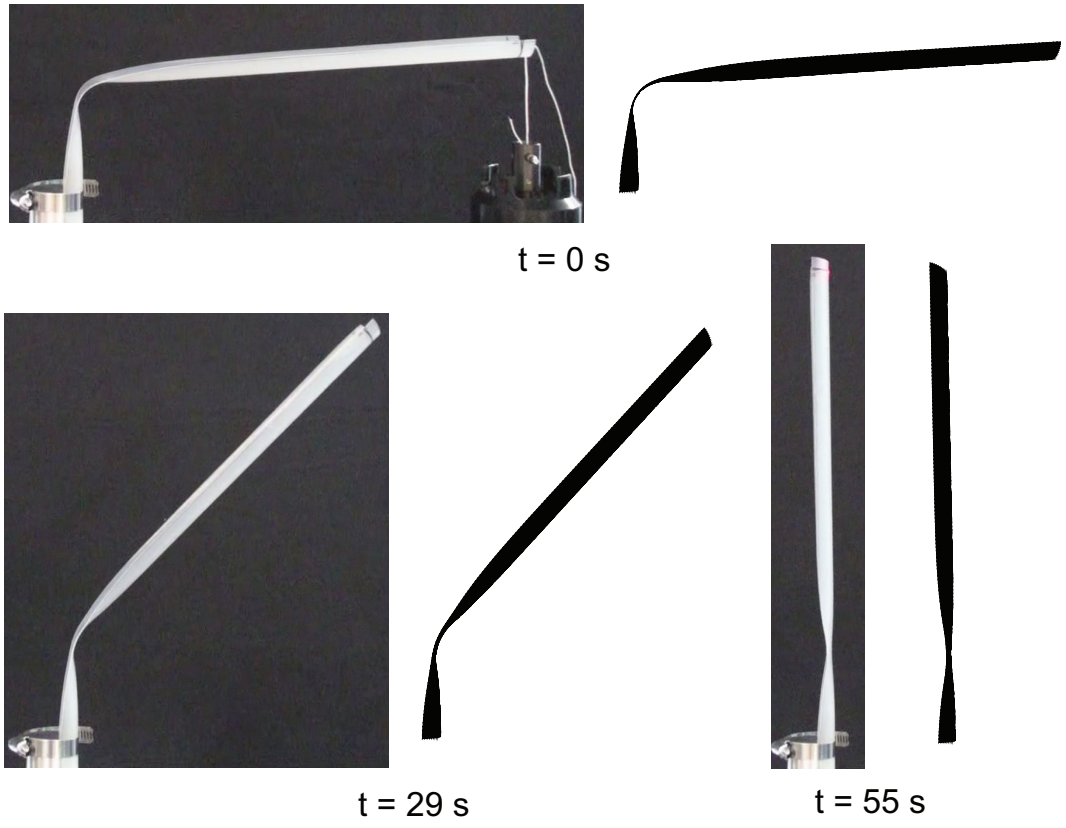

Fig. 23 Comparison of deployed shapes.

The continuous folding, stowage, deployment, and shape recovery processes have been analyzed with a finite element model that incorporates a linear isotropic viscoelastic material model with an experimentally determined relaxation modulus master curve. The material model consists of a six-term Prony series and a Williams-Landel-Ferry type temperature shift function. The finite element model uses shell elements with thickness defined by the measured thickness distribution of the tested specimens to closely capture the instability in load response. The finite element simulations capture the experimentally measured behavior, including the effects of rate and temperature in the nonlinear load-displacement response during folding, load relaxation over an extended stowage duration, short-term deployment as well as long-term shape recovery. Good qualitative and quantitative results in modeling the viscoelastic and nonlinear behavior of shells under quasi-static and dynamic situations have been demonstrated.

In concluding, it should be noted that the numerical simulation techniques presented in this

paper are limited to homogeneous viscoelastic structures. For analyzing viscoelastic composite deployable structures, effective viscoelastic composite properties need to determined and employed in the finite element simulations. Viscoelastic homogenization of fiber reinforced polymer composites and its application to deployable structures is a subject of current study by the authors [26].

Acknowledgments

A preliminary version of this paper was presented at the 52nd AIAA SDM Conference in Denver, CO (AIAA-2011-2022). The authors thank Professor Wolfgang Knauss (California Institute of Technology) for helpful discussions. The award of a doctoral research fellowship from the Croucher Foundation (Hong Kong) to Kawai Kwok is gratefully acknowledged.

References

[1] Rimrott, F., "Storable tubular extensible member: a unique machine element," Machine Design, Vol. 37, 1965, pp. 156–163.

[2] Pellegrino, S., "Large retractable appendages in spacecrafts," Journal of Spacecrafts and Rockets, Vol. 32, 1995, pp. 1006–1014.

[3] Yee, J. and Pellegrino, S., "Composite tube hinges," Journal of Aerospace Engineering, Vol. 18, 2005, pp. 224–231.

[4] Soykasap, O., Pellegrino, S., Howard, P., and Notter, M., "Folding large antenna tape spring," Journal of Spacecrafts and Rockets, Vol. 45, 2008, pp. 560–567.

[5] Mobrem, M. and Adams, D., "Deployment analysis of lenticular jointed antennas onboard the Mars Express Spacecraft," Journal of Spacecrafts and Rockets, Vol. 46, 2009, pp. 394–402.

[6] Adams, D. and Mobrem, M., "Lenticular jointed antenna deployment anomaly and resolution onboard the Mars Express Spacecraft," Journal of Spacecrafts and Rockets, Vol. 46, 2009, pp. 403–408.

[7] Domber, J., Hinkle, J., Peterson, L., and Warren, P., "Dimensional repeatability of an elastically folded composite hinge for deployed spacecraft optics," Journal of Spacecraft and Rockets, Vol. 39, 2002, pp. 646–652.

[8] Soykasap, O., "Deployment analysis of a self-deployable composite boom," Composite Structures, Vol. 89, 2009, pp. 374–381.

[9] Struik, L.C.E., "Physical aging in plastics and other glassy materials," Polymer Engineering and Science, Vol. 17, 1977, pp. 165-173.

[10] Struik, L. C. E., 1978, Physical Aging in Amorphous Polymers and Other Materials, Elsevier, Amsterdam.

[11] Capodagli, J. and Lakes, R., "Isothermal viscoelastic properties of PMMA and LDPE over 11 decades of frequency and time: a test of time-temperature superposition," Rheologica Acta, Vol. 47, 2008, pp. 777–786.

[12] Calladine, C., "The theory of thin shell structures 1888-1988," Proceedings of the Institution of Mechanical Engineers, Vol. 202, 1988, pp. 1–9.

[13] Seffen, K. and Pellegrino, S., "Deployment dynamics of tape springs," Proceedings of the Royal Society of London, Seris A: Mathematical and Physical Sciences, Vol. 455, 1999, pp. 1003–1048.

[14] Kyriakides, S., "Propagating instabilities in structures," Advances in Applied Mechanics, edited by J. Hutchinson and T. Wu, Academic Press, 1994.

[15] Chater, E. and Hutchinson, J., "On the propagation of bulges and buckles," Journal of Applied Mechanics, Vol. 51, 1984, pp. 269–277.

[16] Walker, S.J.I., and Aglietti, G., "Study of the dynamics of three-dimensional tape spring folds," AIAA Journal, Vol. 42(April), 2004, pp. 850-856.

[17] Walker, S.J.I., and Aglietti, G., "Experimental investigation of tape springs folded in three dimensions," AIAA Journal, Vol. 44(January), 2006, pp. 151-159.

[18] Coleman, B. and Noll, W., "Foundations of linear viscoelasticity," Reviews of Modern Physics, Vol. 33, 1961, pp. 239–249.

[19] Flugge, W., Viscoelasticity, Springer-Verlag, New York, 1975.

[20] Ferry, J., Viscoelastic Properties of Polymers, John Wiley and Sons, New York, 3rd ed., 1980.

[21] Tschoegl, N., The Phenomenological Theory of Linear Viscoelastic Behavior, Springer-Verlag, Heidelberg, 1989.

[22] Williams, M., Landel, R., and Ferry, J., "The temperature dependence of relaxation mechanisms of amorphous polymers and other glass-forming liquids," Journal of the American Chemical Society, Vol. 77, 1955, pp. 3701–3707.

[23] Simulia, Abaqus/Standard, Ver. 6.7, Simulia, Providence, 2007.

[24] Lee, S., and Knauss, W., "A note on the determination of relaxation and creep data from ramp tests," Mechanics of Time-Dependent Materials, Vol. 4, 2000, pp. 1–7.

[25] Hilton, H., "Implications and constraints of time-independent Poisson ratios in linear isotropic and anisotropic viscoelasticity," Journal of Elasticity, Vol. 63, 2001, pp. 221–251.

[26] Kwok, K., and Pellegrino, S., "Micromechanical modeling of deployment and shape recovery of

thin-walled viscoelastic composite space structures", 53rd AIAA/ASME/ASCE/AHS/ASC Structures, Structural Dynamics and Materials Conference, 23-26 April 2012, Honolulu, Hawaii. AIAA-2012-1910.